

Simultaneous ground-state cooling of two mechanical modes of a levitated nanoparticle

Received: 25 November 2022

Accepted: 16 January 2023

Published online: 6 March 2023

 Check for updates

Johannes Piotrowski¹, Dominik Windey¹, Jayadev Vijayan¹, Carlos Gonzalez-Ballester^{2,3}, Andrés de los Ríos Sommer⁴, Nadine Meyer⁴, Romain Quidant^{4,5}, Oriol Romero-Isart^{2,3}, René Reimann⁶ & Lukas Novotny¹✉

The quantum ground state of a massive mechanical system is a stepping stone for investigating macroscopic quantum states and building high fidelity sensors. With the recent achievement of ground-state cooling of a single motional mode, levitated nanoparticles have entered the quantum domain. To overcome detrimental cross-coupling and decoherence effects, quantum control needs to be expanded to more system dimensions, but the effect of a decoupled dark mode has so far hindered cavity-based ground-state cooling of multiple mechanical modes. Here, we demonstrate two-dimensional ground-state cooling of an optically levitated nanoparticle. Utilizing coherent scattering into an optical cavity mode, we reduce the occupation numbers of two separate centre-of-mass modes to 0.83 and 0.81, respectively. By controlling the frequency separation and the cavity coupling strengths of the nanoparticle's mechanical modes, we show the transition from 1D to 2D ground-state cooling. This 2D control lays the foundations for quantum-limited orbital angular momentum states for rotation sensing and, combined with ground-state cooling along the third motional axis shown previously, may allow full 3D ground-state cooling of a massive object.

Testing the limits of quantum mechanics as the system size approaches macroscopic scales is one of the grand fundamental and engineering challenges in modern physics^{1–4}. Levitated systems are ideal testbeds for exploring macroscopic quantum physics due to the dynamical and full control over their trapping potential^{5–9}. The motional ground state is the stepping stone for the preparation of quantum states that are delocalized over scales larger than the zero-point motion. Recently, the ground state of the centre-of-mass (COM) motion of a levitated nanoparticle has been reached along a single direction, using both

passive feedback via an optical cavity^{10,11} as well as active measurement-based feedback^{12–14}.

Even though ground-state cooling is typically necessary for preparing macroscopic quantum states, it is not sufficient, as these states are susceptible to decoherence^{5–9}. Cross-coupling between a hot and the ground-state cooled COM mode provides a decoherence channel for the ground-state cooled target mode. Cooling of the hot mode would mitigate this cross-coupling decoherence. Additionally, a second ground-state cooled mode (ancilla mode) would be a powerful tool to

¹Photonics Laboratory, ETH Zurich, Zurich, Switzerland. ²Institute for Quantum Optics and Quantum Information, Austrian Academy of Sciences, Innsbruck, Austria. ³Institute for Theoretical Physics, University of Innsbruck, Innsbruck, Austria. ⁴Nanophotonic Systems Laboratory, ETH Zurich, Zurich, Switzerland. ⁵Quantum Center, ETH Zurich, Zurich, Switzerland. ⁶Quantum Research Center, Technology Innovation Institute, Abu Dhabi, United Arab Emirates. ✉e-mail: lnovotny@ethz.ch

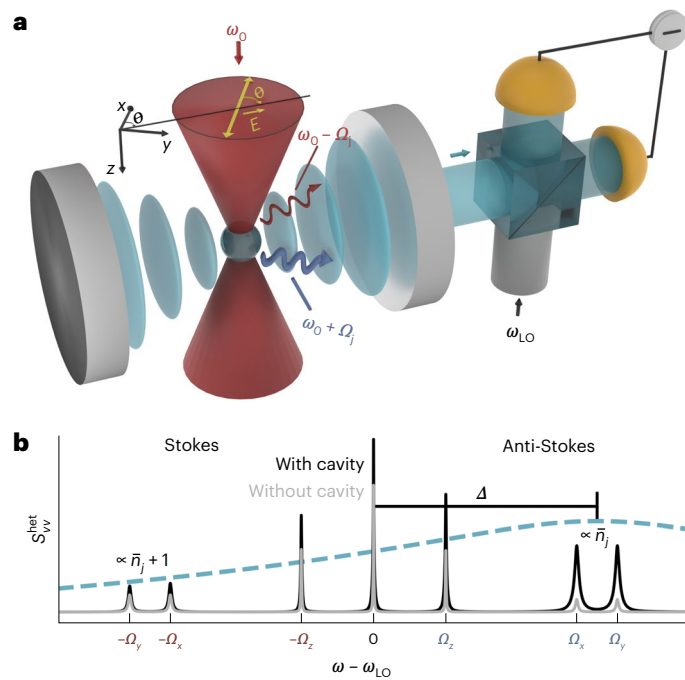


Fig. 1 | Cooling and detection by coherent scattering. **a**, A schematic of the cavity-coupled levitated nanoparticle. The cavity enhances anti-Stokes (blue arrow) over Stokes (red arrow) scattering, leading to cooling of the nanoparticle's mechanical modes. The scattered light at $\omega_0 \pm \Omega_{x,y,z}$ leaks through the high transmission mirror, and interferes with a strong local oscillator at ω_{LO} in a heterodyne detection scheme. The optical tweezers' propagation direction and its polarization define the z and x axis, respectively. The polarization vector is tilted by an angle θ with respect to the cavity axis. **b**, A schematic heterodyne power spectral density (S_{vv}^{het}) of the levitated nanoparticle without the cavity (grey) and filtered by a cavity (black). Six Lorentzian sidebands around the central carrier contain the information of the nanoparticle's three COM modes. The Stokes (anti-Stokes) amplitudes are proportional to $\bar{n}_j + 1$ (\bar{n}_j), which we use for sideband thermometry. The cavity transfer function (dashed blue line) is detuned by Δ from the tweezers' frequency and enhances the anti-Stokes processes, leading to cooling of the mechanical modes.

understand, or even compensate, decoherence effects that influence both ground-state cooled modes. As an example, common dephasing sources (for example, trap frequency noise¹⁵) could be measured in the ancilla mode and then be counteracted in the target mode.

In our levitated particle setup, we achieve simultaneous ground-state cooling of two mechanical modes. We circumvent the key obstacle preventing multimode ground-state cooling in optomechanical systems^{16,17}, namely the effect of the dark mode^{18–21}. The dark hybrid mode is decoupled from the cavity and thus inhibits the efficient cooling of its constituent mechanical modes when they are strongly interacting. We use the unique tunability of levitated systems and adjust the frequency difference between the involved mechanical modes to be larger than the optomechanical coupling rate^{18,22}. Under this constraint, we optimize the optomechanical coupling strength for efficient cooling by coherent scattering^{23,24}.

Experimental setup

A sketch of our optomechanical system is shown in Fig. 1a. Additional information can be found in the Methods. We detect and cool the COM mechanical modes of a single spherical SiO₂ nanoparticle of nominal diameter 143 ± 6 nm and mass 3.4 ± 0.4 fg. The nanoparticle is levitated in high vacuum (pressure of $(5 \pm 4) \times 10^{-9}$ mbar) using optical tweezers at a wavelength of $1,550.0 \pm 0.5$ nm (frequency ω_0) with optical power of 1.20 ± 0.08 W, focused by a high numerical aperture (NA, 0.75) lens. The polarization at the focus is defined by the tilt angle θ between

the major axis of the polarization ellipse and the cavity axis and by the degree of ellipticity. We choose the polarization by tuning a set of waveplates, compensating for the birefringence of our vacuum window and trapping lens. The nanoparticle's reference frame is defined by the tweezers' propagation (z) and polarization (x) axes, as well as the axis orthogonal to the two (y). Strong focusing of the linearly polarized optical tweezers results in non-degenerate, bare mechanical frequencies of the COM motion of $\Omega_{x,y,z}/2\pi = 224 \pm 2, 268 \pm 2, 80 \pm 1$ kHz. The asymmetric cavity consists of two mirrors with different transmission separated by 6.4 ± 0.1 mm, resulting in a linewidth of $\kappa/2\pi = 330 \pm 9$ kHz. The nanoparticle scatters light into the cavity, which leaks through the higher transmission mirror, is combined with a local oscillator ($\omega_{LO}/2\pi = \omega_0/2\pi + 1.5$ MHz) and then split equally onto a balanced photodetector. Heterodyne spectra are calculated as power spectral densities (PSDs) of the balanced photodetector voltage.

Cooling to 2D ground state

Our two-mode ground-state cooling experiment relies on coherent scattering^{25–27}, referring to light being scattered off a polarizable particle and populating an optical cavity. This method has attracted interest as, compared with other cavity cooling schemes, it offers larger optomechanical coupling strengths and reduced phase noise heating²⁴. Here, we exploit coherent scattering for coupling two motional modes of a single nanoparticle to an optical cavity mode^{23,24,28,29}. A harmonically trapped nanoparticle scatters light elastically (Rayleigh) and inelastically (Raman). The Raman processes lead to sidebands in the scattered light spectrum. Figure 1b shows a schematic of the resulting heterodyne spectrum, which illustrates the cooling mechanism of coherent scattering. The positive and negative frequencies correspond to the destruction and creation of a phonon, which are denoted by anti-Stokes and Stokes scattering, respectively. The grey line represents the spectrum of the mechanical oscillations without cavity. We introduce an optical cavity (dashed blue line is the intensity transfer function), whose resonance frequency ω_c is detuned by $\Delta = \omega_c - \omega_0$. As we choose $\Delta \approx (\Omega_x + \Omega_y)/2$, the cavity enhances anti-Stokes relative to Stokes scattering in the spectrum (black line), which reduces the occupation numbers \bar{n}_j ($j = x, y$) of the COM modes. The asymmetry between Stokes and anti-Stokes peaks is additionally influenced by the fact that their scattering rates are proportional to $\bar{n}_j + 1$ and \bar{n}_j , respectively. Taking into account the cavity transfer function, we use the measured asymmetry in the PSDs to extract $\bar{n}_{x,y}$ through a technique called sideband thermometry^{24,30} (Methods). Figure 2a shows the measured heterodyne PSDs normalized to shot noise level. The PSDs contain Stokes and anti-Stokes sidebands of both transversal modes (x and y), simultaneously coupled to the cavity at $\theta = 0.25\pi$, for different cavity detunings Δ . The cooling by coherent scattering becomes more efficient as Δ approaches $(\Omega_x + \Omega_y)/2$, which results in a smaller amplitude and broader width of the sidebands. For each detuning and each COM mode, we fit Lorentzians (lines) of equal widths but independent amplitudes to the Stokes and anti-Stokes sidebands. The asymmetries that we use for sideband thermometry are then given by the ratio of anti-Stokes to Stokes amplitudes. Figure 2b shows the extracted occupation numbers as a function of the cavity detuning. The shaded areas represent simulations based on coupling strengths g_j and heating rates Γ_j , which we extract (Methods) from our data to be $g_x/2\pi = 14.1 \pm 2.7$ kHz, $g_y/2\pi = 15.4 \pm 1.9$ kHz, $\Gamma_x/2\pi = 1.0 \pm 0.4$ kHz and $\Gamma_y/2\pi = 1.0 \pm 0.4$ kHz. We infer the heating rates to be limited by photon recoil (Methods), as they are in good agreement with values calculated from system parameters. For $\Delta/2\pi = 232$ kHz close to $(\Omega_x + \Omega_y)/2$, we reach occupation numbers of $\bar{n}_x = 0.83 \pm 0.10$ and $\bar{n}_y = 0.81 \pm 0.12$, cooling the COM motion into its two-dimensional (2D) quantum ground state.

Transition from 2D to 1D ground-state cooling

We explore the robustness of our cooling scheme to changes of the coupling rates by changing the polarization angle θ of the trapping

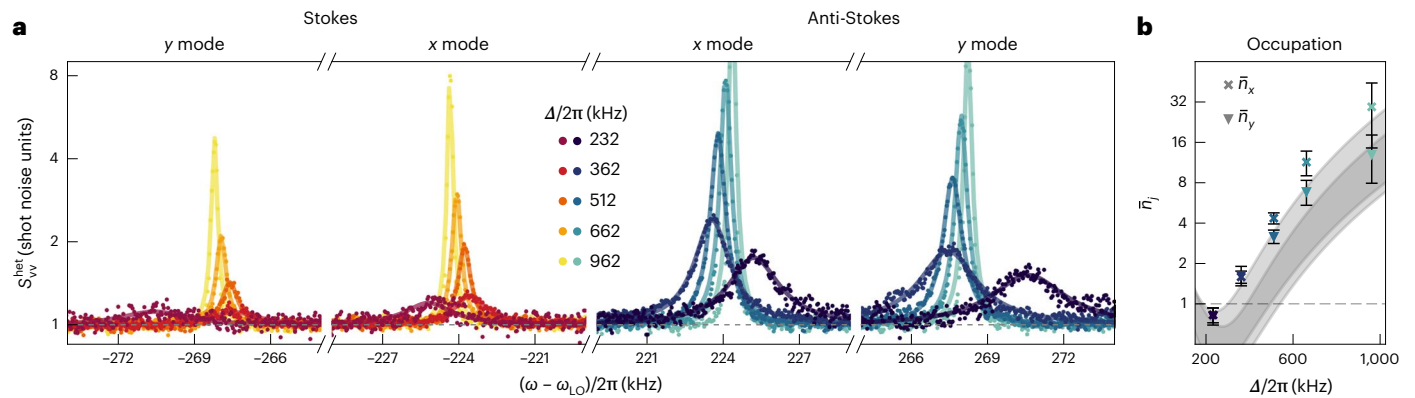


Fig. 2 | Two-mode ground-state cooling. **a**, Heterodyne PSDs of Stokes and anti-Stokes sidebands of x and y modes for different cavity detunings Δ . From Lorentzian fits (lines), the thermal occupation numbers are extracted via sideband thermometry. **b**, Occupation numbers (calculated from fits in **a** with colours matching the detunings) for x and y modes as functions of cavity detuning. For $\Delta/2\pi = 232$ kHz, close to the optimal value $(\Omega_x + \Omega_y)/2$ for

simultaneous cooling, both occupation numbers are cooled below 1 (dashed grey line). Error bars correspond to one s.d. of the fitted asymmetries and the cavity parameters Δ and κ around the calculated occupation numbers. Shaded areas show theoretical estimations of \bar{n}_x (upper) and \bar{n}_y (lower, overlap is darker) based on coupling and heating rates and their uncertainties extracted from the measured PSDs.

light. The linearized optomechanical coupling strengths $g_{x,y}$ for linear polarization have the form $g_x \propto \cos \theta$ and $g_y \propto \sin \theta$ (ref. 28). Figure 3a–d displays anti-Stokes sidebands of x and y modes for different θ at $\Delta/2\pi = 246 \pm 8$ kHz. By tuning θ from 0.25π to 0.5π , we observe the transition from 2D to 1D ground-state cooling. Close to $\theta = 0.5\pi$, the shrinking/rising peak amplitudes indicate the motion along y/x being cooled more/less efficiently owing to larger/smaller coupling strength g_y/g_x . Note that, at $\theta = 0.5\pi$, the x motion is still imprinted in the spectrum of the cavity field and remains cooled. We attribute this to imperfections in the polarization state and in the angular alignment between the optical axes of the trap and cavity. Additionally, small shifts in the frequencies Ω_j for different θ are caused by power drifts of the optical tweezers on the 5% level. The phonon occupations extracted from sideband thermometry $\bar{n}_{x,y}$ are displayed in Fig. 3e. The simulations (shaded areas; Methods) show the increasing and decreasing occupation numbers of the x and y mode, respectively, in agreement with the data. This result is well aligned with the predicted decrease (increase) of $g_x \propto \cos \theta$ ($g_y \propto \sin \theta$) as θ is increased from 0.25π to 0.5π . Experimentally, we find robust two-mode ground-state cooling at $\theta = 0.25\pi$ and 0.33π . Furthermore, we observe our lowest single-mode phonon occupation of $\bar{n}_y = 0.46 \pm 0.05$ paired with a high phonon occupation of $\bar{n}_x = 14 \pm 12$ at $\theta = 0.5\pi$.

Limits of 2D sideband cooling and thermometry

To efficiently cool two COM modes (x, y) of a levitated nanoparticle, several conditions must be met. First, the optical cavity must simultaneously resolve the anti-Stokes sidebands of the x and y modes, that is $|\Omega_y - \Omega_x| \lesssim \kappa \lesssim \Omega_y, \Omega_x$. Further, the system needs to be in the weak coupling regime $|g_j| \ll \kappa$, to prevent hybridization of the cavity and mechanical modes, which hinders efficient cooling³¹. Finally, Ω_x and Ω_y must be sufficiently separated. The x and y modes are cooled by the cavity via a collective bright mechanical mode, while the orthogonal dark mechanical mode is only sympathetically cooled when coupling to the bright mode²². For near-degenerate Ω_x and Ω_y , the dark mode decouples, and this inhibits cooling of its constituent x and y modes (Methods). The condition $|\Omega_y - \Omega_x| \geq |g_j|$ is thus necessary for 2D ground-state cooling^{18,22} (see Methods for details).

The unique in situ tunability of levitated systems allows us to observe the effect of the dark mode decoupling on $\bar{n}_{x,y}$. For a highly focused beam, the shape of the focus spot and thus the resulting trap frequencies are dependent on the incoming polarization³². We change $\Omega_{x,y}$ by tuning the ellipticity of the trapping beam polarization while

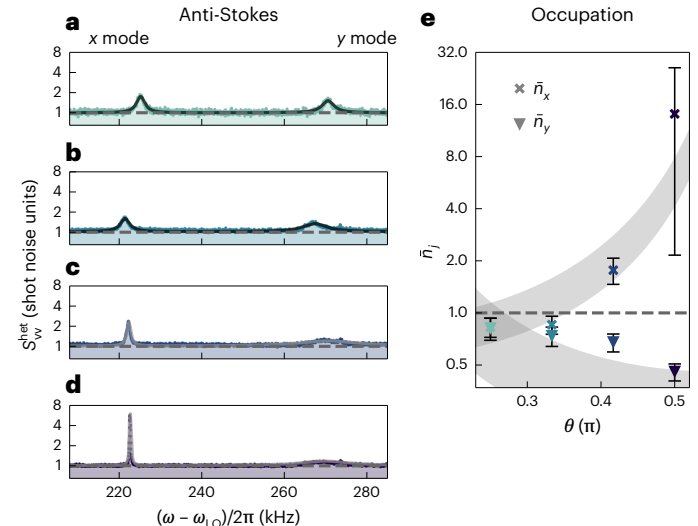


Fig. 3 | Polarization dependence of two-mode cooling. **a–d**, Anti-Stokes sidebands of x and y modes and Lorentzian fits (lines) for different polarization angle θ of 0.25π (**a**), 0.33π (**b**), 0.42π (**c**) and 0.50π (**d**). In **a**, both modes have similar coupling strengths. In **d**, optimal y axis cooling is achieved. **e**, Occupation numbers of x and y modes (colours matching **a–d**) separate for $\theta > 0.25\pi$, transitioning from 2D to 1D cooling. Error bars correspond to one s.d. of the fitted asymmetries and the cavity parameters Δ and κ around the calculated occupation numbers. Shaded areas mark theoretical predictions based on extracted coupling strengths.

keeping $\theta = 0.25\pi$ and $\Delta/2\pi = 257 \pm 11$ kHz. Comparing Fig. 4a and b, we observe that Ω_x and Ω_y approach each other as the polarization changes from linear to elliptical. In Fig. 4b, both modes heat up to $\bar{n}_x = 2.0 \pm 0.4$ and $\bar{n}_y = 2.8 \pm 0.8$ as weak coupling of the dark mode inhibits cooling. As we polarize the tweezers circularly for Fig. 4c, x and y peaks merge and we are unable to extract individual occupation numbers by conventional sideband thermometry.

We further theoretically test the validity of extracting phonon numbers by sideband thermometry using a full quantum model²⁸ (Methods). We first calculate the true phonon occupation \bar{n}_j^{model} for $j = x, y$. Then, using the same model, we calculate PSDs of the heterodyne detection and perform sideband thermometry on them to extract \bar{n}_j . We define the systematic error $\delta\bar{n}_j = |(\bar{n}_j^{\text{model}} - \bar{n}_j)/\bar{n}_j^{\text{model}}|$ and show

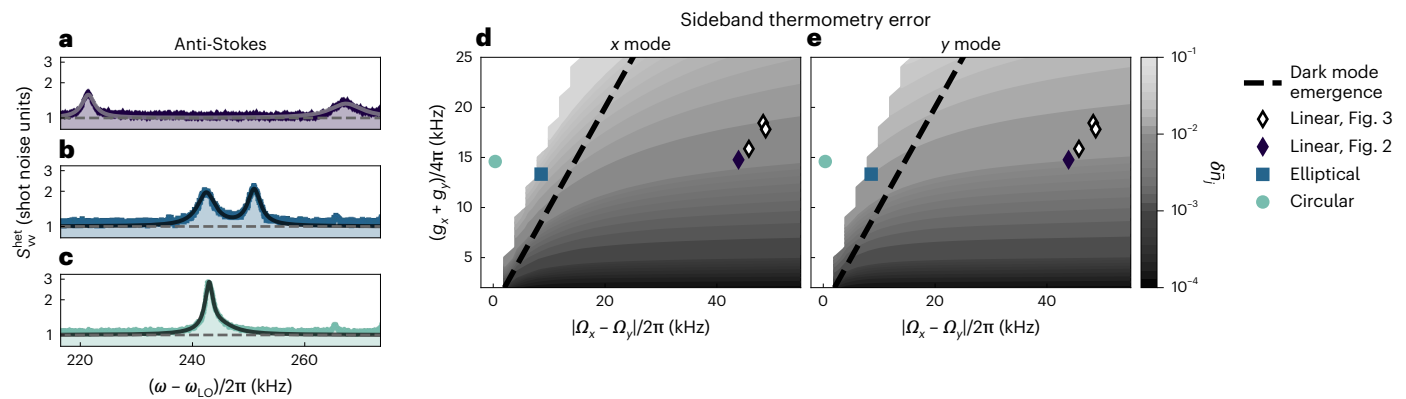


Fig. 4 | Limits of 2D sideband cooling. **a–c**, Anti-Stokes sidebands of x and y modes for linear (**a**), elliptical (**b**) and circular (**c**) ellipticity in the trap's polarization. The separation between peaks $\Omega_y - \Omega_x$ decreases with increasing ellipticity. In **b**, cross-coupling increases the occupation numbers to $\bar{n}_x = 2.1 \pm 0.4$ and $\bar{n}_y = 2.8 \pm 0.8$. Circular polarization causes degenerate peaks

in **c**, **d**, **e**. The relative error of x (**d**) and y (**e**) occupation extracted by sideband thermometry versus the real phonon number. Parameter pairs of measurements in Figs. 2 and 3b–d as well as **b** and **c** are marked by points. The dark mode decoupling prevents efficient cooling for $\Omega_y - \Omega_x < (g_x + g_y)/2$ (black line), and sideband thermometry becomes impossible for degenerate peaks (white area).

the result in Fig. 4d,e. Mostly we find that \bar{n}_j underestimates \bar{n}_j^{model} . In the weak coupling regime and for well-separated COM mode frequencies, $\delta\bar{n}_j$ is negligible. For stronger coupling and constant mode spacing, hybridization between optical and mechanical modes becomes more impactful and $\delta\bar{n}_j$ increases. At constant coupling rate, the error also increases as the mechanical frequencies approach degeneracy and the effect of the dark mode gains importance. We cannot perform 2D sideband thermometry for degenerate peaks, which occurs at small mode spacing and large coupling strength (Fig. 4d,e white areas). Finally we display the estimated errors for all measurements presented in Figs. 2–4. These errors of our sideband thermometry method are marginal, for Fig. 2 only about 1%, which confirms that we have achieved two-mode ground-state cooling.

Conclusions

We have simultaneously prepared two out of three COM modes of a levitated particle in their ground state with residual occupation numbers of $\bar{n}_x = 0.83$ and $\bar{n}_y = 0.81$. With respect to the optical axis of the tweezers, our cooling scheme controls the transversal degrees of freedom, resulting in two important implications.

First, together with the demonstrated ground-state cooling along the tweezers' axis^{12–14}, 3D COM quantum control is within experimental reach. Demonstrating 3D ground-state cooling would be an important step towards full control of large systems at the quantum limit.

Second, control over transversal COM motion implies control of the orbital angular momentum along the tweezers' axis, given by $\hat{L}_z = \hat{x}\hat{p}_y - \hat{y}\hat{p}_x$, where (\hat{x}, \hat{y}) and (\hat{p}_x, \hat{p}_y) are the transverse position and momentum vector operator, respectively. As the particle's transversal motion is in a thermal state, the variance of the corresponding angular momentum is given by $\langle \hat{L}_z^2 \rangle / \hbar^2 = (\bar{n}_x + 1/2)(\bar{n}_y + 1/2)(\Omega_x/\Omega_y + \Omega_y/\Omega_x) - 1/2$. With our occupation numbers and trap frequencies, we find $\sqrt{\langle \hat{L}_z^2 \rangle} \approx 1.7 \hbar$. We have therefore prepared our system close to an angular momentum eigenstate along z ($\langle \hat{L}_z^2 \rangle = 0$) with $\langle \hat{L}_z \rangle = 0$. This opens the door to realizing protocols combining 2D ground-state cooling with coherently pumped orbital angular momentum³³ to stabilize a state with large orbital angular momentum $\langle \hat{L}_z \rangle \gg \hbar$ and quantum-limited variance. Those minimally fluctuating high orbital angular momentum states ('quantum orbits') would be promising not only for fundamental studies of low-noise and massive high angular momentum states but also for becoming building blocks of a gyroscope with quantum-limited performance.

Online content

Any methods, additional references, Nature Portfolio reporting summaries, source data, extended data, supplementary information, acknowledgements, peer review information; details of author contributions and competing interests; and statements of data and code availability are available at <https://doi.org/10.1038/s41567-023-01956-1>.

References

- Bose, S., Jacobs, K. & Knight, P. L. Scheme to probe the decoherence of a macroscopic object. *Phys. Rev. A* **59**, 3204–3210 (1999).
- Leggett, A. J. Testing the limits of quantum mechanics: motivation, state of play, prospects. *J. Phys. Condens. Matter* **14**, R415–R451 (2002).
- Marshall, W., Simon, C., Penrose, R. & Bouwmeester, D. Towards quantum superpositions of a mirror. *Phys. Rev. Lett.* **91**, 130401 (2003).
- Schlosshauer, M. *Decoherence and the Quantum-to-Classical Transition* (Springer, 2008).
- Romero-Isart, O. et al. Large quantum superpositions and interference of massive nanometer-sized objects. *Phys. Rev. Lett.* **107**, 020405 (2011).
- Romero-Isart, O. Quantum superposition of massive objects and collapse models. *Phys. Rev. A* **84**, 052121 (2011).
- Neumeier, L., Ciampini, M. A., Romero-Isart, O., Aspelmeyer, M. & Kiesel, N. Fast quantum interference of a nanoparticle via optical potential control. Preprint at *arXiv* <https://doi.org/10.48550/arXiv.2207.12539> (2022).
- Weiss, T., Roda-Llodes, M., Torrontegui, E., Aspelmeyer, M. & Romero-Isart, O. Large quantum delocalization of a levitated nanoparticle using optimal control: applications for force sensing and entangling via weak forces. *Phys. Rev. Lett.* **127**, 023601 (2021).
- Gonzalez-Ballester, C., Aspelmeyer, M., Novotny, L., Quidant, R. & Romero-Isart, O. Levitodynamics: levitation and control of microscopic objects in vacuum. *Science* **374**, eabg3027 (2021).
- Delić, Uroš. et al. Cooling of a levitated nanoparticle to the motional quantum ground state. *Science* **367**, 892–895 (2020).
- Ranfagni, A., Børkje, K., Marino, F. & Marin, F. Two-dimensional quantum motion of a levitated nanosphere. *Phys. Rev. Res.* **4**, 033051 (2022).
- Tebbenjohanns, F., Mattana, M. L., Rossi, M., Frimmer, M. & Novotny, L. Quantum control of a nanoparticle optically levitated in cryogenic free space. *Nature* **595**, 378–382 (2021).

13. Magrini, L. et al. Real-time optimal quantum control of mechanical motion at room temperature. *Nature* **595**, 373–377 (2021).
14. Kamba, M., Shimizu, R. & Aikawa, K. Optical cold damping of neutral nanoparticles near the ground state in an optical lattice. *Optics Express* **30**, 26716 (2022).
15. Gehm, M. E., O’Hara, K. M., Savard, T. A. & Thomas, J. E. Dynamics of noise-induced heating in atom traps. *Phys. Rev. A* **58**, 3914–3921 (1998).
16. Cattiaux, D. et al. A macroscopic object passively cooled into its quantum ground state of motion beyond single-mode cooling. *Nat. Commun.* **12**, 6182 (2021).
17. Liu, Jin-Yu et al. Ground-state cooling of multiple near-degenerate mechanical modes. *Phys. Rev. A* **105**, 053518 (2022).
18. Genes, C., Vitali, D. & Tombesi, P. Simultaneous cooling and entanglement of mechanical modes of a micromirror in an optical cavity. *N. J. Phys.* **10**, 095009 (2008).
19. Shkarin, A. B. et al. Optically mediated hybridization between two mechanical modes. *Phys. Rev. Lett.* **112**, 013602 (2014).
20. Ockeloen-Korppi, C. F. et al. Sideband cooling of nearly degenerate micromechanical oscillators in a multimode optomechanical system. *Phys. Rev. A* **99**, 023826 (2019).
21. Lai, Deng-Gao et al. Nonreciprocal ground-state cooling of multiple mechanical resonators. *Phys. Rev. A* **102**, 011502 (2020).
22. Toroš, M., Delić, Uroš., Hales, F. & Monteiro, T. S. Coherent-scattering two-dimensional cooling in levitated cavity optomechanics. *Phys. Rev. Res.* **3**, 023071 (2021).
23. Windey, D. et al. Cavity-based 3D cooling of a levitated nanoparticle via coherent scattering. *Phys. Rev. Lett.* **122**, 123601 (2019).
24. Delić, Uroš. et al. Cavity cooling of a levitated nanosphere by coherent scattering. *Phys. Rev. Lett.* **122**, 123602 (2019).
25. Hechenblaikner, G., Gangl, M., Horak, P. & Ritsch, H. Cooling an atom in a weakly driven high-q cavity. *Phys. Rev. A* **58**, 3030–3042 (1998).
26. Vuletić, V. & Chu, S. Laser cooling of atoms, ions, or molecules by coherent scattering. *Phys. Rev. Lett.* **84**, 3787–3790 (2000).
27. Hosseini, M., Duan, Y., Beck, K. M., Chen, Yu-Ting & Vuletić, V. Cavity cooling of many atoms. *Phys. Rev. Lett.* **118**, 183601 (2017).
28. Gonzalez-Ballester, C. et al. Theory for cavity cooling of levitated nanoparticles via coherent scattering: master equation approach. *Phys. Rev. A* **100**, 013805 (2019).
29. Ranfagni, A. et al. Vectorial polaritons in the quantum motion of a levitated nanosphere. *Nat. Phys.* **17**, 1120–1124 (2021).
30. Leibfried, D., Blatt, R., Monroe, C. & Wineland, D. Quantum dynamics of single trapped ions. *Rev. Mod. Phys.* **75**, 281–324 (2003).
31. Aspelmeyer, M., Kippenberg, T. J. & Marquardt, F. Cavity optomechanics. in *Quantum Science and Technology* (Springer, 2014).
32. Novotny, L. and Hecht, B. *Principles of Nano-Optics* 2nd edn (Cambridge Univ. Press, 2012).
33. Svak, V. et al. Transverse spin forces and non-equilibrium particle dynamics in a circularly polarized vacuum optical trap. *Nat. Commun.* **9**, 5453 (2018).

Publisher’s note Springer Nature remains neutral with regard to jurisdictional claims in published maps and institutional affiliations.

Open Access This article is licensed under a Creative Commons Attribution 4.0 International License, which permits use, sharing, adaptation, distribution and reproduction in any medium or format, as long as you give appropriate credit to the original author(s) and the source, provide a link to the Creative Commons license, and indicate if changes were made. The images or other third party material in this article are included in the article’s Creative Commons license, unless indicated otherwise in a credit line to the material. If material is not included in the article’s Creative Commons license and your intended use is not permitted by statutory regulation or exceeds the permitted use, you will need to obtain permission directly from the copyright holder. To view a copy of this license, visit <http://creativecommons.org/licenses/by/4.0/>.

© The Author(s) 2023

Methods

Setup

A detailed view of the experimental setup is shown in Extended Data Figs. 1 and 2. To keep our cavity free of contaminants and at vacuum conditions (below 10^{-2} mbar) at all times, we load nanoparticles (SiO_2 -F-L3205-23, 143 ± 6 nm nominal diameter; microParticles GmbH) in a separate loading chamber (not drawn in Extended Data Fig. 1) using a nebulizer (Omron). The loading tweezers are mounted on a movable arm, and its light is frequency shifted by acousto-optic modulator (AOM)3 by 80 MHz to avoid interference. After loading, we seal and evacuate the loading chamber to 1×10^{-2} mbar and move the loading tweezers into the cavity chamber. We use two photodetectors and the loading tweezers' nanopositioner (SmarAct GmbH) to align the focal points of loading and science tweezers. Initially, we measure the intensity of light passing by the particle on PD_{BR} to roughly align the two foci, while the science tweezers are still turned off. Afterwards, we gradually increase the power of the science tweezers and measure the light coupling into the fibre of the loading tweezers and shining on PD_L. Eventually, we turn down and up the power in the trapping and science tweezers, respectively, to transfer the nanoparticle to the science tweezers. Thereafter, the science chamber is sealed off and pumped down to 5×10^{-9} mbar by using a combination of a turbomolecular pump and an ion-getter pump.

The cavity with linewidth $\kappa/2\pi = 330$ kHz, finesse $\mathcal{F} = 70$ k and focal spot waist $w_c = 48 \pm 5$ μm is built from a low and high finesse mirror (specified finesse of coatings of 37k and 126k) with a radius of curvature of 10 mm and cavity length of $L = 6.4$ mm. The absorption A and transmission T of the low (high) finesse coatings are 4 and 79 ppm (5 and 20 ppm), respectively. We lock the cavity to the TEM₁₀ mode of the cavity to avoid interference with light scattered off the particle into the TEM₀₀ mode. The necessary frequency shift $\omega_{10} - \omega_{00}$ of approximately 8 GHz is generated by AOM1 and electro-optic modulator (EOM)1 to obtain the lock beam sent into the cavity. We define the cavity detuning $\Delta = \omega_c - \omega_0$ with respect to the cavity resonance frequency ω_c of the TEM₀₀ mode. The backscattered light is collected on a photodiode (PD_{PDH}) to generate the error signal for a Pound–Drever–Hall lock³⁴ of the cavity length. The small sidebands necessary for the error signal are generated by EOM2 at 23 MHz.

Detuning calibration

To perform accurate sideband thermometry, we need to compensate for the effect of cavity filtering of the motional sidebands. For a known detuning Δ and linewidth κ , we can readily calculate the cavity-induced asymmetry at a mode frequency Ω_j by assuming a Lorentzian filter function³⁵:

$$A_j^{(\text{cav})} = \frac{\kappa^2 + 4(\Delta + \Omega_j)^2}{\kappa^2 + 4(\Delta - \Omega_j)^2}.$$

In our experiments, the particle scatters light into the TEM₀₀ of the optical cavity, while the cavity is locked to the TEM₁₀ mode. The difference of the two TEM mode frequencies is very sensitive to drifts of the cavity length between experiments. Thus, we need to calibrate the detuning of the cavity with respect to the science tweezers. As a particle-independent measure, we temporarily send a calibration laser through the cavity before performing cooling experiments. This laser has sidebands modulated by an electro-optic modulator (EOM3) at 300 kHz and higher harmonics, which are filtered by the detuned cavity and then detected in our heterodyne scheme (Extended Data Fig. 3a). We extract the asymmetry of these three sidebands and the z-peak of the particle motion while tuning the cavity lock frequency with EOM1. In Extended Data Fig. 3b, we fit the Lorentzian cavity filter function to the measured sideband asymmetry to extract the linewidth and calibrate the detuning Δ . The linewidth agrees with an independent

measurement of $\kappa/2\pi = 330$ kHz. The s.d. values for Δ in Fig. 2b are below 3 kHz, and therefore the error bars are smaller than the markers.

Sideband thermometry

For extracting the phonon occupation from measured heterodyne signals, we rely on the different scaling of Stokes and anti-Stokes scattering processes. As the latter requires the presence of a phonon, its scattering rate scales with the average phonon number n , while the Stokes scattering rate scales with $n + 1$. This leads to an asymmetry of the anti-Stokes and Stokes sidebands dependent on the occupation number:

$$A_j^{(n)} = \frac{\bar{n}_j}{\bar{n}_j + 1}.$$

The total asymmetry of the PSD at the frequency Ω_j

$$A_j = \frac{S_{vv}(\Delta_{10} + \Omega_j)}{S_{vv}(\Delta_{10} - \Omega_j)} = A_j^{(n)} A_j^{(\text{cav})}$$

is the product of the thermal asymmetry $A_j^{(n)}$ and the cavity/induced asymmetry $A_j^{(\text{cav})}$. Given both, we can calculate the average occupation number

$$\bar{n}_j = \frac{A_j}{A_j^{(\text{cav})} - A_j}.$$

To access the thermal asymmetry, we assume a Lorentzian shape of the motional sidebands

$$S_{jj}(\Omega) \approx \frac{a_j}{2\pi} \frac{\frac{\gamma_j}{2}}{(\Omega - \Omega_j)^2 + \left(\frac{\gamma_j}{2}\right)^2},$$

with amplitude a_j , width γ_j and centre frequency Ω_j . Our fitting function

$$F = S_{xx,(\text{AS})} + S_{xx,(\text{S})} + S_{yy,(\text{AS})} + S_{yy,(\text{S})} + S_{\text{SN}}$$

lets us extract four values for a_j , γ_j and Ω_j , one for each Stokes and anti-Stokes sideband of mode $j = x, y$, and gives $A_j^{(n)} = a_{j,\text{AS}}/a_{j,\text{S}}$. We require $\gamma_{j,\text{AS}} = \gamma_{j,\text{S}}$ and $\Omega_{j,\text{AS}} = -\Omega_{j,\text{S}}$. The shot noise level S_{SN} is extracted for each PSD in a region far away from any spectral features to account for small drifts in the local oscillator power. We normalize all spectra to the shot noise level. For the error bars, we propagate the s.d. of the fitted amplitudes a_j and the cavity parameters Δ and κ .

Quantum model

The Hamiltonian describing coherent scattering is²⁸

$$\frac{\hat{H}_{\text{CS}}}{\hbar} = \Delta \hat{a}^\dagger \hat{a} + \sum_{j=x,y,z} \Omega_j \hat{b}_j^\dagger \hat{b}_j - \sum_{j=x,y,z} (g_j \hat{a}^\dagger + \text{h.c.}) (\hat{b}_j^\dagger + \hat{b}_j),$$

with \hat{a} (\hat{a}^\dagger) being the photon annihilation (creation) operator, \hat{b}_j (\hat{b}_j^\dagger) the phonon annihilation (creation) operator along motional axis $j = x, y, z$, and h.c. the Hermitian conjugate. This interaction allows to cool the COM motion along all three axes, as has been demonstrated experimentally^{36,37}. The linearized optomechanical coupling strengths g_j for linear polarization are given by

$$\begin{bmatrix} g_x \\ g_y \\ g_z \end{bmatrix} = -\frac{G_0}{2} \begin{bmatrix} k_c x_{\text{zpf}} \sin \phi \cos \theta \\ k_c y_{\text{zpf}} \sin \phi \sin \theta \\ -ik_c z_{\text{zpf}} \cos \phi \end{bmatrix} \quad (1)$$

with $k_c = 2\pi/\lambda_c$ the cavity wavevector, $[x_{\text{zpf}}, y_{\text{zpf}}, z_{\text{zpf}}] = \sqrt{\frac{\hbar}{2m\Omega_{x,y,z}}}$ the zero-point fluctuations (zpf) along each axis and $\phi = 2\pi y_0/\lambda_c$, with y_0 being the particle position along the cavity axis and $y_0 = \lambda_c/4$

corresponding to an intensity minimum of the cavity standing wave. The rate $G_0 = \alpha E_0 \sqrt{\frac{\omega_c}{2\hbar\epsilon_0 V_c}} \mathbf{e}_x \cdot \mathbf{e}_\alpha$ contains the particle polarizability $\alpha = 4\pi\epsilon_0 R^3 \frac{n^2-1}{n^2+2}$ (with n , the refractive index of the particle, R its radius and ϵ_0 the vacuum permittivity), the trap electric field amplitude $E_0 = \sqrt{\frac{4P}{\pi\epsilon_0 c w_x w_y}}$ with $w_{x,y}$ the trap waists at the focus, and the cavity parameters, namely the mode volume $V_c = \pi w_c^2 L_c / 4$, the cavity waist w_c , the cavity length L_c , the frequency $\omega_c = 2\pi c / \lambda_c$ and the unit vector along the cavity axis \mathbf{e}_α . Note that the vector dot product $\mathbf{e}_x \cdot \mathbf{e}_\alpha$ introduces an additional dependence on the trap polarization angle $\propto \cos\theta$, which hinders the possibility of coupling solely the x motional mode to the cavity.

The quantum state of the cavity–nanoparticle system is given by its density matrix $\hat{\rho}$, which obeys the dynamical equation²⁸

$$\begin{aligned} \frac{d}{dt}\hat{\rho} = & -\frac{i}{\hbar} [H_{CS}, \hat{\rho}] + \kappa [\hat{a}\hat{\rho}\hat{a}^\dagger - \{\hat{a}^\dagger\hat{a}, \hat{\rho}\}/2] \\ & - \sum_{j=x,y,z} \frac{\Gamma_j}{2} [\hat{b}_j + \hat{b}_j^\dagger, [\hat{b}_j + \hat{b}_j^\dagger, \hat{\rho}]] \\ & + \frac{\gamma}{4} \sum_{j=x,y,z} [\hat{b}_j + \hat{b}_j^\dagger, \{\hat{b}_j - \hat{b}_j^\dagger, \hat{\rho}\}], \end{aligned} \quad (2)$$

where $\{\cdot\}$ denotes the anticommutator, γ is the friction rate due to gas damping and the heating rates $\Gamma_j = \Gamma_j^{(r)} + \Gamma_j^{(g)}$ contain a contribution from gas molecules

$$\Gamma_j^{(g)} = \gamma \frac{k_B T}{\hbar \Omega_j} \quad (3)$$

and a contribution from laser recoil heating

$$\begin{bmatrix} \Gamma_x^{(r)} \\ \Gamma_y^{(r)} \\ \Gamma_z^{(r)} \end{bmatrix} = \frac{\pi}{15\hbar\epsilon_0} \left(\frac{\alpha E_0}{2\pi} \right)^2 k_0^5 \begin{bmatrix} x_{zpf}^2 \\ 2y_{zpf}^2 \\ 7z_{zpf}^2 \end{bmatrix}. \quad (4)$$

To obtain analytical expressions, we simplify the model by making two assumptions. First, friction due to gas molecules is negligible, which at the pressures used for this work can be checked to be a good approximation^{28,38}. This amounts to neglecting the friction term in the master equation, namely the last line in equation (2). Note that the associated heating rate $\Gamma_j^{(g)} \gg \gamma$ is not neglected. Second, the particle equilibrium position is at the intensity minimum of the cavity mode ($\phi = \pi/2$). This is the case for all measurements in this work within an accuracy of 1 nm. At this position, the couplings $g_{x,y}$ are simultaneously maximized while the z mode becomes uncoupled. Under these approximations, the system is reduced to a three-mode system including only the cavity mode and the x and y motional modes, whose steady-state properties can be computed analytically (see below).

Within this three-mode approximation, we can explain the dark-mode effect. The Hamiltonian can be cast in the form

$$\frac{\hat{H}_{CS}}{\hbar} = \Delta \hat{a}^\dagger \hat{a} + \sum_{j=\pm} \omega_j \hat{b}_j^\dagger \hat{b}_j + G_\pm (\hat{b}_+^\dagger \hat{b}_- + \text{h.c.}) - (g_x \hat{a}^\dagger + \text{h.c.}) (\hat{b}_+^\dagger + \hat{b}_+). \quad (5)$$

Here, we have changed basis in the x – y subspace to define two collective mechanical modes, namely the bright and dark modes

$$\hat{B}_+ \equiv \frac{g_x \hat{b}_x + g_y \hat{b}_y}{g_\pm}, \quad \hat{B}_- \equiv \frac{g_y \hat{b}_x - g_x \hat{b}_y}{g_\pm}, \quad (6)$$

with the total coupling rate $g_\pm = \sqrt{g_x^2 + g_y^2}$. The corresponding mechanical frequencies of bright and dark mode read

$$\omega_+ = \frac{\Omega_x g_x^2 + \Omega_y g_y^2}{g_\pm^2}, \quad \omega_- = \frac{\Omega_x g_y^2 + \Omega_y g_x^2}{g_\pm^2}. \quad (7)$$

According to the Hamiltonian in equation (5), the cavity couples directly only to the bright mode and can thus only cool this mode. The dark mode can be only sympathetically cooled through its coupling to the bright mode, which has a rate

$$G_\pm = \frac{g_x g_y}{g_\pm^2} (\Omega_x - \Omega_y). \quad (8)$$

In the optimal 2D cooling configuration, $\Gamma_x \approx \Gamma_y \equiv \Gamma$ and $g_x \approx g_y \equiv g$, so that the above rates simplify to $g_\pm \approx \sqrt{2}|g|$ and $G_\pm \approx (\Omega_x - \Omega_y)/2$. For 2D ground-state mechanical cooling, both the bright and dark states must be cooled at a rate higher than their respective heating rate. For the bright state, this reduces to the standard optomechanical condition $\frac{8g^2}{\kappa} > \Gamma$. As the dark state is cooled by the bright state and not by the cavity, for the dark state the condition reads

$$\frac{4G_\pm^2}{(8g^2/\kappa)} = \frac{\kappa(\omega_x - \omega_y)^2}{8g^2} > \Gamma. \quad (9)$$

Combining both conditions, we arrive to the inequality

$$\sqrt{\frac{\Gamma\kappa}{8}} < g < |\omega_x - \omega_y| \sqrt{\kappa/(8\Gamma)}, \quad (10)$$

which defines a ‘Goldilocks zone’ for 2D cooling³⁹. In particular, if the mechanical modes are close to degeneracy, the cooling of the dark mode is not efficient enough for it to reach the ground state. This in turn limits the steady-state occupations of the original modes x and y , which are now limited by the thermal dark-mode occupation, $\langle \hat{b}_{x,y}^\dagger \hat{b}_{x,y} \rangle \sim \langle \hat{b}_-^\dagger \hat{b}_- \rangle$. Note that, in typical coherent scattering experiments, $\sqrt{\kappa/8\Gamma}$ is on the order of 1–10, so that the the right-hand side of the Goldilocks condition reduces to the condition $|\omega_x - \omega_y| \geq |g|$ given in the main text.

Extracting coupling and heating rates

Within the two above assumptions (negligible friction and z motion uncoupled), the heterodyne power spectral density can be analytically calculated. The heterodyne PSD, after subtraction of the noise floor and normalization to it, can be written as⁴⁰

$$S_{\text{het}}(\omega) = \kappa [S_c(\delta_{L0} - \omega) + S_c(\omega + \delta_{L0})] \quad (11)$$

with $\delta_{L0} = \omega_{L0} - \omega_0$. It is expressed in terms of the cavity PSD

$$S_c(\omega) = \int_{-\infty}^{\infty} \frac{ds}{2\pi} e^{-i\omega s} \langle \hat{a}^\dagger(0) \hat{a}(s) \rangle_{ss}, \quad (12)$$

where the subscript ‘ss’ indicates the steady state. We compute the two-time correlator using the quantum regression theorem²⁸, obtaining the following analytical expression:

$$\begin{aligned} S_c(\omega) = & \frac{16 \left[4g_x^4 \kappa \Omega_x^2 (\omega^2 - \Omega_y^2)^2 \right. \\ & + g_x^2 \Omega_x (\omega^2 - \Omega_y^2) \left[\Gamma_x \Omega_x (\omega^2 - \Omega_y^2) (4(\Delta - \omega)^2 + \kappa^2) \right. \\ & + 8g_y^2 \kappa \Omega_y (\omega^2 - \Omega_x^2) \left. \right] \\ & + g_y^2 \Omega_y^2 (\omega^2 - \Omega_x^2)^2 \left. \left(\Gamma_y (4(\Delta - \omega)^2 + \kappa^2) + 4g_x^2 \kappa \right) \right]}{\pi \left[4\Delta^2 (\omega^2 - \Omega_x^2) (\omega^2 - \Omega_y^2) \right. \\ & + 16\Delta (g_x^2 \Omega_x (\omega^2 - \Omega_y^2) + g_y^2 \Omega_y (\omega^2 - \Omega_x^2)) \\ & + (\kappa^2 - 4\omega^2) (\omega^2 - \Omega_x^2) (\omega^2 - \Omega_y^2) \left. \right]^2 \\ & + 16\kappa^2 \omega^2 (\omega^2 - \Omega_x^2)^2 (\omega^2 - \Omega_y^2)^2}. \end{aligned} \quad (13)$$

To extract from our data the experimental values for $g_{x,y}$ and $\Gamma_{x,y}$, we fit equation (11) to our time traces while setting κ and Δ to the values from our calibration.

Calculated heating rates

Using equations (3) and (4), we calculate the heating rates of x and y motion using the parameters given in the main text and $T = 300$ K, $n_r = 1.439$, $w_x = 1.023 \mu\text{m}$, $w_y = 0.856 \mu\text{m}$ and $\gamma = 4,812 \text{ Hz} \times p_{\text{gas,mbar}}$, with $p_{\text{gas,mbar}}$ the gas pressure in mbar. At $p_{\text{gas,mbar}} = 5 \times 10^{-9}$, we obtain $\Gamma_x^{(g)} = 2\pi \times 0.053 \text{ kHz}$, $\Gamma_y^{(g)} = 2\pi \times 0.045 \text{ kHz}$, $\Gamma_x^{(r)} = 2\pi \times 0.825 \text{ kHz}$ and $\Gamma_y^{(r)} = 2\pi \times 1.379 \text{ kHz}$. The total heating rate is thus dominated by photon recoil, $\Gamma_{x,y}^{(g)} \ll \Gamma_{x,y}^{(r)}$ and $\Gamma_{x,y}^{(r)}$ agrees with the values extracted from our measured PSDs. We heavily suppress heating due to phase noise, as we position the particle in the cavity node and use an ultra-low phase noise laser source⁴¹. Note that the stated pressure reading of $p_{\text{gas}} = 5 \times 10^{-9}$ mbar is measured close to the ion-getter pump. The actual pressure at the position of the nanoparticle could be larger. $\Gamma_{x,y}^{(g)}$ becomes comparable to $\Gamma_{x,y}^{(r)}$ at $p_{\text{gas,mbar}} \approx 10^{-7}$, suggesting that the gas pressure near the nanoparticle is lower than this value.

Error in sideband thermometry

The effects of optical–mechanical mode hybridization and the decoupling of the dark mode modify the spectra measured through the cavity. As conventional sideband thermometry does not take these effects into account when estimating occupation numbers, the method is affected by a systematic error. To obtain this error, we theoretically calculate the occupation \bar{n}_j estimated via sideband thermometry by numerically computing the maxima of equation (13) and compensating for the cavity asymmetry as detailed above. We then compare this result with the exact phonon occupations $\bar{n}_j^{\text{model}} = \langle \hat{b}_j^\dagger \hat{b}_j \rangle$ within our approximations (negligible friction and z motion uncoupled). For the results in Fig. 4d,e, we fix $\Delta = 2\pi \times 240 \text{ kHz}$, $g_x = g_y = g$, $\Omega_x = \Delta - \delta$ and $\Omega_y = \Delta + \delta$, and sweep over the parameters δ and g . At each point (that is, for each value of $\Omega_{x,y}$), the corresponding heating rates Γ_j are calculated from equations (3) and (4).

Data availability

Source data for Figs. 2–4 and Extended Data Fig. 3 are available in the ETH Zurich Research Collection (<https://doi.org/10.3929/ethz-b-000591807>). All other data that support the plots within this paper and other findings of this study are available from the corresponding author upon reasonable request.

References

34. Drever, R. W. P. et al. Laser phase and frequency stabilization using an optical resonator. *Appl. Phys. B* **31**, 97–105 (1983).
35. Delić, Uroš. et al. Cooling of a levitated nanoparticle to the motional quantum ground state. *Science* **367**, 892–895 (2020).

36. Windey, D. et al. Cavity-based 3D cooling of a levitated nanoparticle via coherent scattering. *Phys. Rev. Lett.* **122**, 123601 (2019).
37. Delić, Uroš. et al. Cavity cooling of a levitated nanosphere by coherent scattering. *Phys. Rev. Lett.* **122**, 123602 (2019).
38. Ranfagni, A., Børkje, K., Marino, F. & Marin, F. Two-dimensional quantum motion of a levitated nanosphere. *Phys. Rev. Res.* **4**, 033051 (2022).
39. Toroš, M., Delić, Uroš., Hales, F. & Monteiro, T. S. Coherent-scattering two-dimensional cooling in levitated cavity optomechanics. *Phys. Rev. Res.* **3**, 023071 (2021).
40. Bowen, W. P. & Milburn, G. J. *Quantum Optomechanics* (Taylor & Francis, 2015).
41. Meyer, N. et al. Resolved-sideband cooling of a levitated nanoparticle in the presence of laser phase noise. *Phys. Rev. Lett.* **123**, 153601 (2019).

Acknowledgements

We thank our colleagues E. Bonvin, L. Devaud, M. Frimmer, J. Gao, V. van der Laan, M. L. Mattana, A. Militaru, M. Rossi, N. Carlon Zambon and J. Zielinska for input and discussions. L.N., O.R.-I. and R.Q. acknowledge support by the European Research Council (grant no. 951234, Q-Xtreme) and by the European Union's Horizon 2020 research and innovation programme (grant no. 863132, iQLev).

Author contributions

J.P. and D.W. conducted the experiments with equal contribution, supported by J.V. C.G.-B. and O.R.-I. performed the theoretical modelling, A.d.L.R.S., N.M. and R.Q. conceptualized the setup with R.R. and L.N., who directed the project.

Funding

Open access funding provided by Swiss Federal Institute of Technology Zurich.

Competing interests

The authors declare no competing interests.

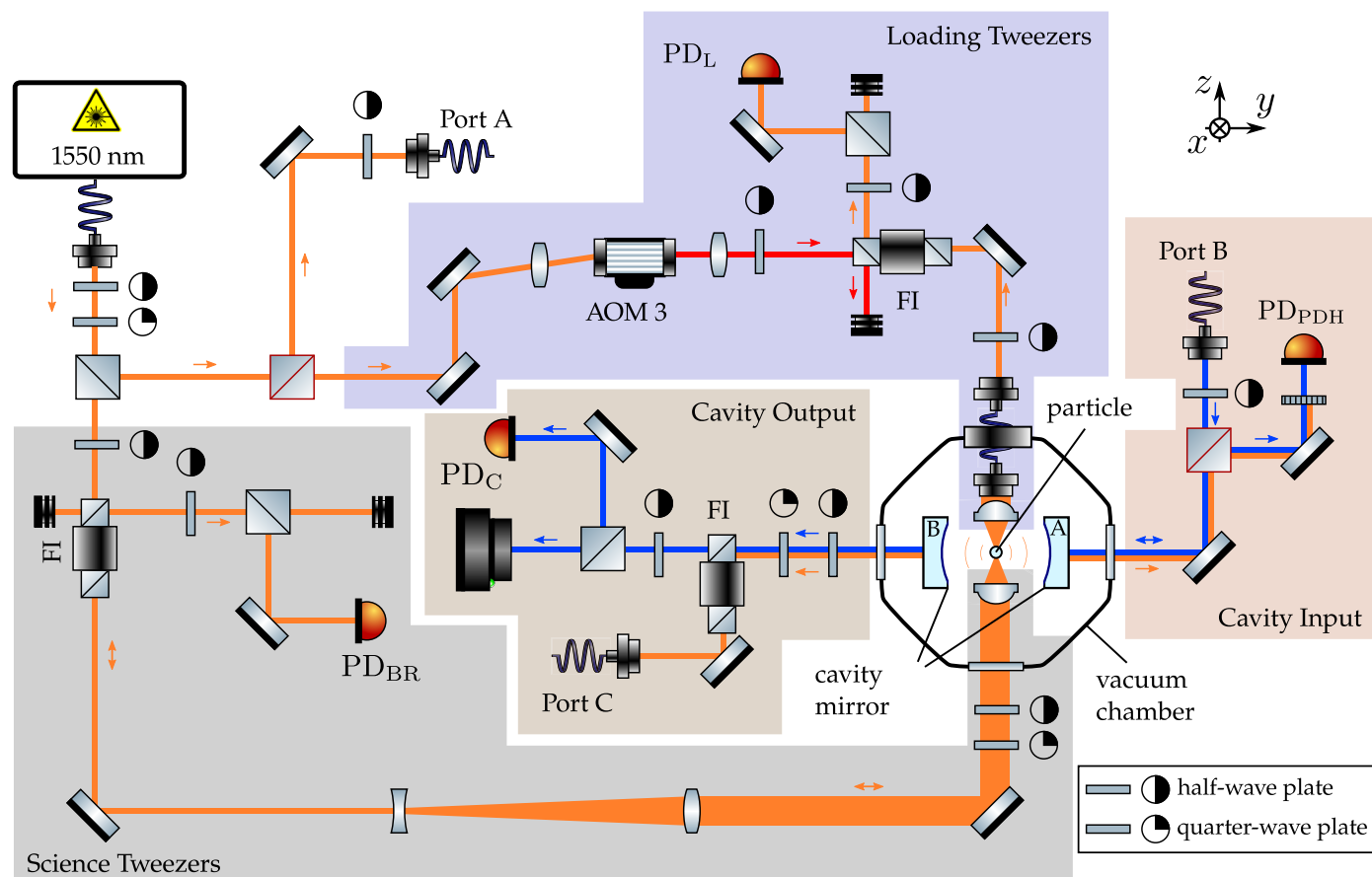
Additional information

Extended data is available for this paper at <https://doi.org/10.1038/s41567-023-01956-1>.

Correspondence and requests for materials should be addressed to Lukas Novotny.

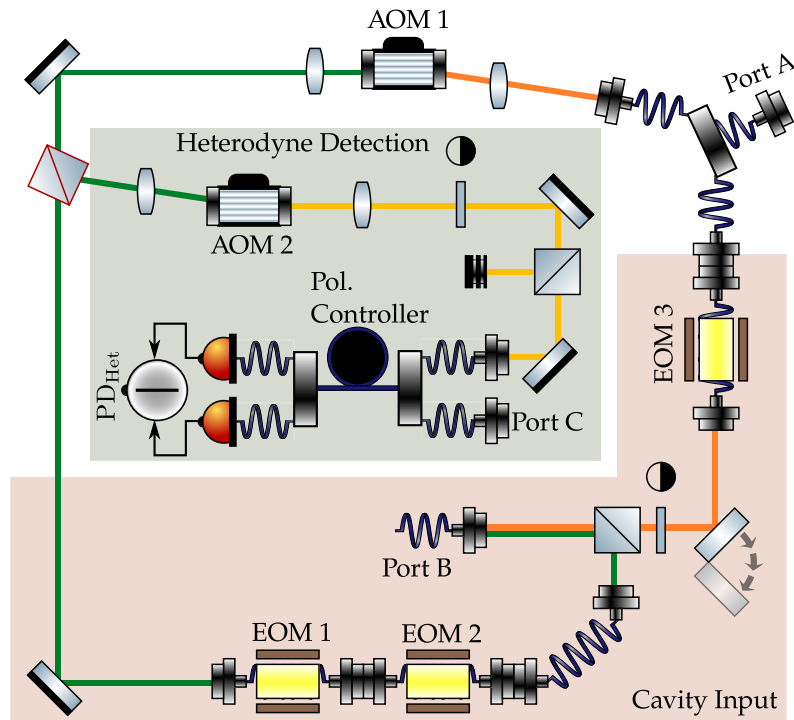
Peer review information *Nature Physics* thanks the anonymous reviewers for their contribution to the peer review of this work.

Reprints and permissions information is available at www.nature.com/reprints.



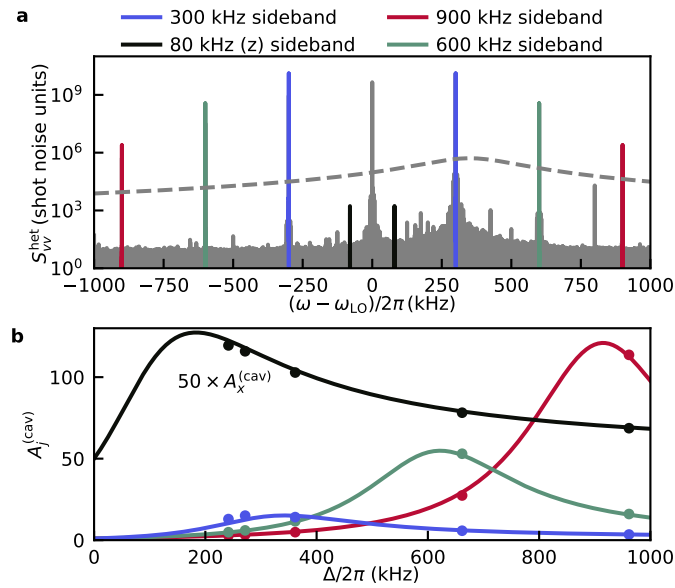
Extended Data Fig. 1 | Core setup for particle trapping, transfer and detection. To simplify the sketch, we show components of the detection setup and cavity lock on a separate sketch in Extended Data Fig. 2. We link the ports as indicated by the letter. All beam splitters with a black (red) outline are polarising (non-polarising) beam splitters and components labeled FI are Faraday isolators. All beams are derived from a *NKT Photonics E15* 1550 nm laser. In the sketched configuration (particle loaded in science tweezers), the half wave plate in the loading tweezers' section is set to dump all power at the input of a FI. Initially, while loading the particle, the loading tweezers are positioned in a separate vacuum chamber (not shown) and the full power is used to trap a particle. The photodetector PD_L is used to monitor the trapping process. After aligning the loading tweezers with the science tweezers we rotate the half wave plate in front

of the FI in the science tweezers' section to turn on the science tweezers. At the same time, we rotate the half-wave plate in the loading tweezers section, to turn off the loading tweezers and transfer the particle. From port B we feed in a beam to lock the cavity length by using the signal of the photodetector PD_{PDH} . To reduce noise on the detector we cross polarise the beam with respect to the tweezers and use a polariser to filter out the particle scattered light. On the opposite side of the cavity we use a photodiode to monitor the lock quality PD_C and an infrared camera to image the cavity mode. The mirror on the right is the high finesse mirror, therefore most of the particle scattered light leaks through the left mirror. We feed the light that leaks out of the cavity to port C to detect it with the heterodyne setup.



Extended Data Fig. 2 | Constituent setup for particle detection, cavity locking and calibration. All components are sketched as described in Extended Data Fig. 1. Light from the core setup enters from the top right through port A. We drive AOM1 (+ 1st order) and AOM2 (− 1st order) at $2\pi \times 80$ MHz and $2\pi \times 78.5$ MHz, resulting in a local oscillator detuning $\Delta_{10} = 1.5$ MHz. As we lock to the TEM_{10} mode of the cavity, we use AOM1 and EOM1 to derive a beam at

frequency close to $\omega_{10} - \omega_{00}$ (the difference of the resonance frequencies of TEM_{10} and TEM_{00}). On the opposite side of the cavity input section, we modulate sidebands on the calibration beam before combining it with the lock beam. We implement a flip mirror to prevent the calibration beam from entering port B and consequently the cavity, while doing measurements.



Extended Data Fig. 3 | Detuning calibration by known sidebands.

a, EOM-modulated sidebands of the calibration laser at 900 kHz (red), 600 kHz (green) and 300 kHz (blue), as well as the uncooled z-peak at 80 kHz (black) are filtered by the cavity transfer function (grey dashed line). **b**, We fit (lines) the

detuning-dependent, expected cavity-induced asymmetry $A_j^{(cav)}$ to the measured asymmetries at all four sidebands. The asymmetry of the x-peak is multiplied by 50 for visibility.